Four-Dimensional Elastic Light-Scattering Fingerprints as Preneoplastic Markers in the Rat Model of Colon Carcinogenesis

HEMANT K. ROY,* YANG LIU,† RAMESH K. WALI,* YOUNG L. KIM,† ALEXEI K. KROMINE,† MICHAEL J. GOLDBERG,* and VADIM BACKMAN†

*Department of Internal Medicine, Evanston-Northwestern Healthcare, Evanston, Illinois; and †Biomedical Engineering Department, Northwestern University, Evanston, Illinois

Background & Aims: **Identification of preneoplastic changes in histologically normal epithelium (the "field effect") could provide a powerful screening tool for colorectal cancer. However, to date, reliable detection has not been possible. We have recently developed a new generation of optical technology, 4-dimensional elastic light-scattering fingerprinting (4D-ELF), which enables us to probe the nanoscale/microscale architecture of living cells. We therefore investigated whether 4D-ELF would be able to identify preneoplastic changes in the colonocytes of the azoxymethane (AOM)-treated rat model of colon carcinogenesis.** ***Methods:*** **Forty-eight Fisher 344 rats were randomized to either 2 weekly injections of AOM or saline. Animals were killed 2–20 weeks after the second injection of AOM. Colons were removed and subjected to 4D-ELF analysis, with a subset undergoing assessment of aberrant crypt foci (ACF). All AOM-treated animals were compared with age-matched saline-treated controls.** ***Results:*** **AOM-induced ACF became apparent at approximately 4–6 weeks and continued to increase over time. ACF were predominantly located in the distal colon. At 2 weeks (before development of ACF), there were marked changes in a number of 4D-ELF signatures. The relevance to carcinogenesis of these 4D-ELF–detected microarchitectural abnormalities is supported by their spatial and temporal correlation with subsequent development of ACF. All changes reported were highly statistically significant.** ***Conclusions:*** **We show that probing the nanoscale cellular architecture with 4D-ELF provided an unprecedented tool for detecting the earliest stages of colon carcinogenesis. Future studies are necessary to explore the clinical applicability of this technology and elucidate the biological determinants of these microarchitectural changes.**

Colorectal neoplasms are the second-leading cause of cancer deaths in the United States, underscoring the public health imperative for developing novel strategies to combat this malignancy.[1] Screening has been shown to decrease colorectal cancer mortality by both identifying lesions at an early, potentially curable stage and also through prevention of colorectal cancer development by targeting the precursor lesions, the adenomatous polyps.[2] However, there are many barriers to widespread implementation of these strategies, including patient noncompliance, discomfort, economic constraints, resource availability, and risk of complications.[3] Indeed, most eligible subjects do not receive any type of screening for colorectal cancer, which is in marked contrast to screening rates for other common malignancies (e.g., breast, prostate).[3,4]

Therefore, it is clear that improved screening methodologies are essential to decrease the number of fatalities due to colorectal cancer. Many screening techniques are designed to exploit the "field effect" of colon carcinogenesis, the proposition that the genetic/environmental milieu that results in neoplasia in one region should be detectable throughout the mucosa.[5] For instance, the detection of distal adenomatous polyps by flexible sigmoidoscopy is commonly used to risk-stratify patients for proximal neoplasia and, hence, the need for colonoscopy.[6] Furthermore, rectal aberrant crypt foci (ACF) have been shown to accurately predict the occurrence of colon adenomas and carcinomas.[7] From a cellular perspective, apoptosis in the uninvolved mucosa (both basal[8] and bile salt induced[9]) has been shown to be a reliable marker for colonic neoplasia. Several biochemical markers have also been evaluated, including colonic protein kinase C activity[10] and mucus disaccharide content.[11] Although all of these markers have shown a statistically significant correlation between rectal assays and colonic neoplasia (i.e., the field effect), their performance characteristics are

Abbreviations used in this paper: ACF, aberrant crypt foci; AOM, azoxymethane; 4D-ELF, 4-dimensional elastic light-scattering fingerprinting; LSS, light-scattering spectroscopy; PCA, principal component analysis; PC1, principal component 1.

0016-5085/04/$30.00
doi:10.1053/j.gastro.2004.01.009

suboptimal for clinical practice. Novel techniques to detect the field effect are therefore urgently needed.

There are several lines of evidence that subtle perturbations in colonic microarchitecture may be a manifestation of the field effect. For instance, in the "transitional mucosa" (histologically normal epithelium adjacent to colon cancer), a number of abnormalities in the cell nuclei have been noted, including changes in parameters such as total optical density, nuclear area, chromatin texture, and coarseness.[12–14] Although microarchitectural alterations may serve as an excellent marker of the field effect of colon carcinogenesis, current technology does not allow its practical and accurate detection. Advances in biomedical optics have the potential of enabling real-time in vivo assessment of intracellular structure. We, in conjunction with others, have pioneered light-scattering spectroscopy (LSS) for identifying cellular atypia.[15–17] The clinical applicability of this technology is indicated by our demonstration that dysplasia in Barrett's esophagus can be accurately identified using an endoscopically compatible LSS probe.[18] Moreover, LSS was shown to be able to detect early stages of colorectal carcinogenesis.[17,19] However, this relatively basic first-generation technology relies on detection of altered nuclear size and chromatin content. Therefore, it may be less adept at detecting the more subtle microarchitectural changes of the field effect and thus less useful in screening for colorectal cancer.

Light-scattering signals are extremely rich and complicated, thus having the potential for yielding unprecedented insights into the microarchitectural organization of the cell. Light-scattering signals from tissue surfaces depend not only on the size, shape, and internal organization of intracellular structures but also on the position of these objects in relation to the cell itself or a larger organelle (the immediate surrounding milieu of solid particles such as proteins). To realize the full promise of light scattering, we developed 4-dimensional elastic light-scattering fingerprinting (4D-ELF), a new generation of optical technology.[20] This technology allows us to obtain quantitative information about biological structures without the need for tissue biopsy, fixation, staining, or other processing. 4D-ELF enables probing tissue organization at scales from tens of nanometers to microns, thus encompassing a spectrum of structures ranging from macromolecular complexes to whole cells. Indeed, this provides information about objects 20–50 times smaller than can be detected by conventional microscopy. Thus, the light-scattering fingerprints provide a heretofore-unattainable insight into the architecture of living tissue at the nanoscale organizational level.

The objective of this study was to assess whether 4D-ELF would be able to detect the field effect of colon carcinogenesis. In the present studies, we tested 4D-ELF in the azoxymethane (AOM)-treated rat, a well-validated model of colorectal carcinogenesis that recapitulates many of the important morphologic, genetic, and cellular alterations found in human colon cancer.[21] We show that 4D-ELF is able to accurately identify alterations in the colonic mucosa at a far earlier stage than any previously described markers. Furthermore, these changes correlated well with the carcinogenic progression in this model.

Materials and Methods

Overview of 4D-ELF

LSS is based on the principle that the intensity of light elastically scattered (i.e., without change in wavelength) from a tissue is a function of the composition of both light absorbers and scatterers within the tissue. Light absorption is governed by molecules such as hemoglobin, whereas scattering is determined by the sizes and densities of space-occupying structures including cell organelles and macromolecular complexes. An extension of LSS, 4D-ELF allows acquisition of light-scattering data in several dimensions, thus providing unprecedented insights into tissue composition. The dimensions of 4D-ELF are (1) wavelength of light, (2) the scattering angle (i.e., the angle between the backward direction and the direction of the propagation of scattered light), (3) azimuthal angle of scattering (i.e., the angle between the incident light polarization and the projection of the direction of the scattered light propagation onto the plane in which the incident electric field oscillates), and (4) polarization of scattered light. Thus, in 4D-ELF, scattered light is analyzed as a function of its wavelength in dimension 1, direction of propagation in dimensions 2 and 3, and polarization in dimension 4.

Light-Scattering Fingerprinting

To obtain the 4D-ELF data, we have developed an advanced light-scattering instrument as previously described.[20] Briefly, our instrument (Figure 1) consists of 2 components: the light delivery system (used to illuminate a tissue site approximately 1 mm in diameter) and the collection system (which gathers light scattered by the tissue). In the delivery system, the broadband light emitted by a xenon light source (Oriel Inc., Strafford, CT) was collimated by means of the lamp condenser and a lens system and was linearly polarized using a polarizer. Thus, a collimated linearly polarized beam of broadband light was delivered onto a tissue surface. For each wavelength, the tissue scatterers the incident light in a wide range of directions and polarization states. This scattered light was recorded using the light collection system; the scattered light was transmitted through an analyzing polarizer that selected the desired polarization of the scattered light (see following text), a Fourier lens (Newport, Inc., Irvine, CA)

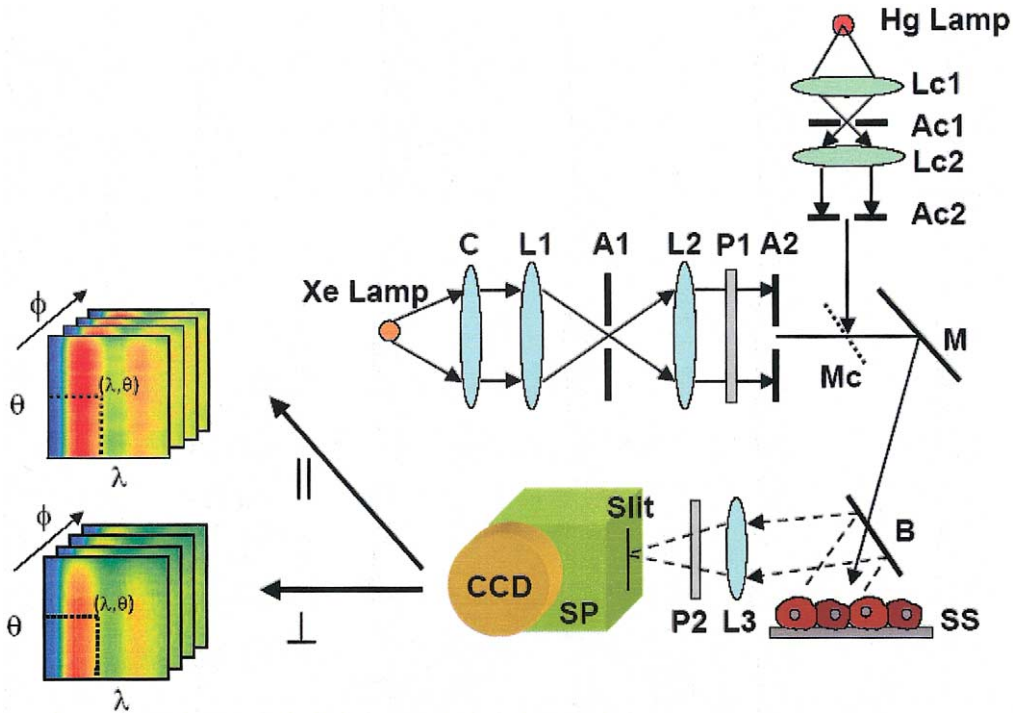

Figure 1. Schematic representation of the 4D-ELF instrument: Xe, xenon lamp; Hg, mercury lamp; C, condenser; L, lenses; A, apertures; P, polarizers; M, mirrors; B, beam splitter; SS, sample stage; SP, spectrograph; CCD, charge-coupled device camera; Lc, calibration lenses; Ac, calibration apertures.

positioned one focal distance from a tissue surface, and the imaging spectrometer (SpectraPro-150; Acton Research Corp., Acton, MA), which was positioned one focal distance from the Fourier lens and coupled to the charge-coupled device (CoolSnapHQ; Roper Scientific, Inc., Trenton, NJ), which served as the scattered light detector. The Fourier lens projects an angular distribution of the scattered light onto the entrance slit of the spectrometer. This light was further diverted by the spectrometer according to its spectral content, now in the direction orthogonal to the slit, and projected onto the charge-coupled device. Thus, the instrument recorded a matrix of the distribution of scattered light intensity for various wavelengths (from 400 to 700 nm) and angles of scattering (within $\pm 5°$ from the backward direction; here the angle of scattering is defined as the angle between the direction opposite to the direction of propagation of the incident light and the direction of propagation of the scattered light). In this matrix, one axis corresponds to the wavelength of light and the other to the angle of scattering for a fixed polarization and the azimuth of scattering. The azimuth of scattering is selected by rotating the polarizer in the delivery arm of the system. The combination of the linear polarizer in the delivery arm of the system and the analyzing polarizer allows measurement of the intensity of 2 independent components of the light scattered from the tissue: scattered light polarized along the direction of polarization of the incident light (co-polarized component $I_{\|}$) and the scattered light polarized orthogonally to the polarization of the incident light (the cross-polarized component $I_{\perp}$). To compensate for non-uniform spectral profile of the light source and other artifacts, the light-scattering intensity maps were normalized to a reflectance standard (Ocean Optics, Inc., Dunedin, FL). The instrument was calibrated and tested using conventional protocol with physical tissue models,[20] which consisted of suspensions of polystyrene microspheres of different sizes ranging from 0.2 to 10 μm. The light-scattering data recorded in these experiments were found to be in excellent agreement with the predictions of Mie theory, which provides exact solution to the light scattering by spheres.

The polarization-sensitive detection has an important advantage over conventional unpolarized measurements by allowing penetration depth selectivity. Most biological tissues are relatively turbid. Light propagation in such media is dominated by the multiple scattering from tissue structures located within several millimeters of the tissue surface, which in the case of colon tissue typically includes both the mucosa and submucosa. The single scattering collected by means of polarization gating is primarily contributed by scatterers located close to the tissue surface and therefore particularly sensitive to the properties of the superficial tissues (e.g., the epithelia).[20,22,23] As shown by our previous work,[20] the differential polarization signal ($\Delta I = I_{\|} - I_{\perp}$) is primarily contributed by the most superficial tissue structures located within the first 30–50 μm of the tissue surface, which typically includes the epithelial cell layer. The co-polarized signal $I_{\|}$, diffuse reflectance signal $I_{\|}+I_{\perp}$, and the cross-polarized signal $I_{\perp}$ provide information about progressively deeper tissues (up to several millimeters below the surface). Light scattering and absorption by red blood cells may alter the differential polarization signals ΔI, which characterize tissue nanoarchitecture and microarchitecture. Because differential polarized signals are superpositions of single scattering contributions from various tissue scatterers within the superficial tissue, the signals from red blood cells in rat tissue samples were subtracted from the unprocessed light-scattering spectra by fitting the red

blood cell signals to ΔI using a previously established algorithm.[20]

Although unpolarized diffuse reflectance tissues have previously been studied,[24–29] the information obtained regarding tissue structures is averaged over several photon transport paths (approximately several millimeters), which does not allow characterization of epithelial and near-epithelial tissues. On the other hand, polarization gated measurements, as reported here, can provide principally new information about changes in organization of epithelial cells, which is crucial for detection of the initial stages of carcinogenesis.[20,22,23,30]

Analysis of Light-Scattering Fingerprints

Briefly, 4-dimensional light-scattering fingerprints contain the wealth of information about tissue microarchitecture and nanoarchitecture.[20] A number of light-scattering signatures can be linked to specific properties of cell architecture, including the size distribution of intraepithelial nanoscale and microscale structures (from ~30–40 to 800 nm) and the fractal dimension of the cell structure at supramicro scales (greater than ~1 μm).[20,31,32] The combination of these measures enables quantitative characterization of epithelial architecture in a wide range of scales, from tens of nanometers to microns.

To obtain the complete size distribution of subcellular structures at each tissue site, the spectra computationally simulated using Mie theory were fit to the differential polarization tissue spectra for a given scattering angle and azimuth of scattering using the conventional least-squares minimization algorithm.[33] In each fitting, several types of size distributions (normal, log-normal, or uniform) were assumed. We found that the spectra recorded by our instrument for scattering angles within ±5° from the backward direction had spectral behavior similar to an inverse power-law, which is consistent with our previous results[31] as well as results obtained by other groups.[32,34] Our studies confirmed that if the sizes of scatterers are widely distributed, as is characteristic of biological tissues, the log-normal or power-law size distributions provide fits superior to those obtained using a normal or uniform size distribution. This agrees well with our observations as well as those of other groups.[31,32,34–36] The log-normal probability distribution depends on 2 parameters: its mean (i.e., the mean size of tissue structures giving rise to the scattering signal) and the standard deviation of particle sizes, which characterizes particle size variability. Therefore, we varied these parameters to minimize the χ^2. The size-sensitivity studies showed that the differential polarization spectra are primarily sensitive only to scatterers with sizes ranging from 40 to 800 nm. Therefore, these limits provide the range of validity of the size distributions obtained using the fitting algorithm.

We also used principal component analysis (PCA) as one of the tools for data analysis.[37] For PCA, the light-scattering spectra were averaged over scattering angles from −5° to 5°. Each spectrum was preprocessed by mean scaling.[38] A data matrix was created in which each row of the matrix contained the preprocessed spectrum measurement and each column contained the preprocessed scattering intensity at each wavelength. The scores of all principal components were calculated using Matlab statistics toolbox software version 6.5 (The Mathworks, Inc., Natick, MA).

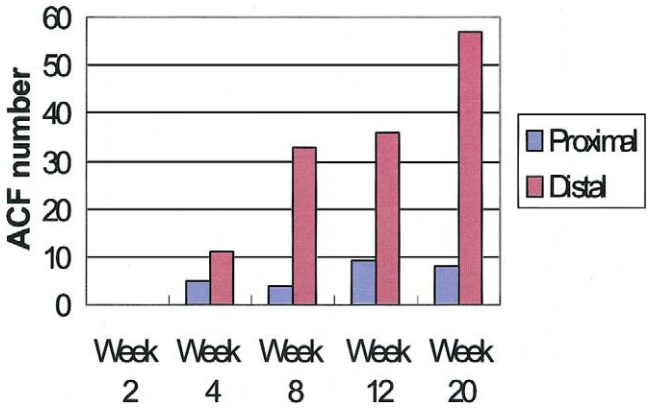

Figure 2. Temporal progression of ACF in a subset of AOM-treated rats. ACF were detected predominantly in the distal colon, and there was a linear progression over time. There were markedly fewer ACF in the proximal colon, especially at the early time points.

Animals

All animal studies were performed in accordance with the institutional Animal Care and Use Committee of Evanston-Northwestern Healthcare. Forty-eight male Fisher 344 rats (150–200 g) were randomized equally to groups that received either 2 weekly intraperitoneal injections of AOM (15 mg/kg) (Sigma Chemical Co., St. Louis, MO) or saline. Rats were fed standard chow and were killed at various times after the second injection (2, 4, 5, 6, 8, 12, and 20 weeks). Colons were removed, flushed with phosphate-buffered saline, and divided into equal proximal and distal segments. 4D-ELF analysis was performed on fresh tissue. Quantitation of ACF was performed on a subset of animals using methods previously described.[39] Briefly, after fixation overnight in 10% buffered formalin, colon segments were stained for 2 minutes in 0.2% methylene blue (Sigma Chemical Co.), rinsed in phosphate-buffered saline, and examined with a dissecting microscope. ACF (defined as a foci containing ≥2 crypts) were scored by an observer blinded to treatment.

Results

Assessment of ACF

We analyzed the number of ACF on a subset of animals in this study to correlate this well-validated biomarker of colon carcinogenesis to the 4D-ELF readings. ACF were detectable at week 4 and progressively increased in both number and complexity over the course of the experiment. As shown in Figure 2, there was a marked distal predominance in ACF. Although proximal ACF occurred, these required longer to develop and were

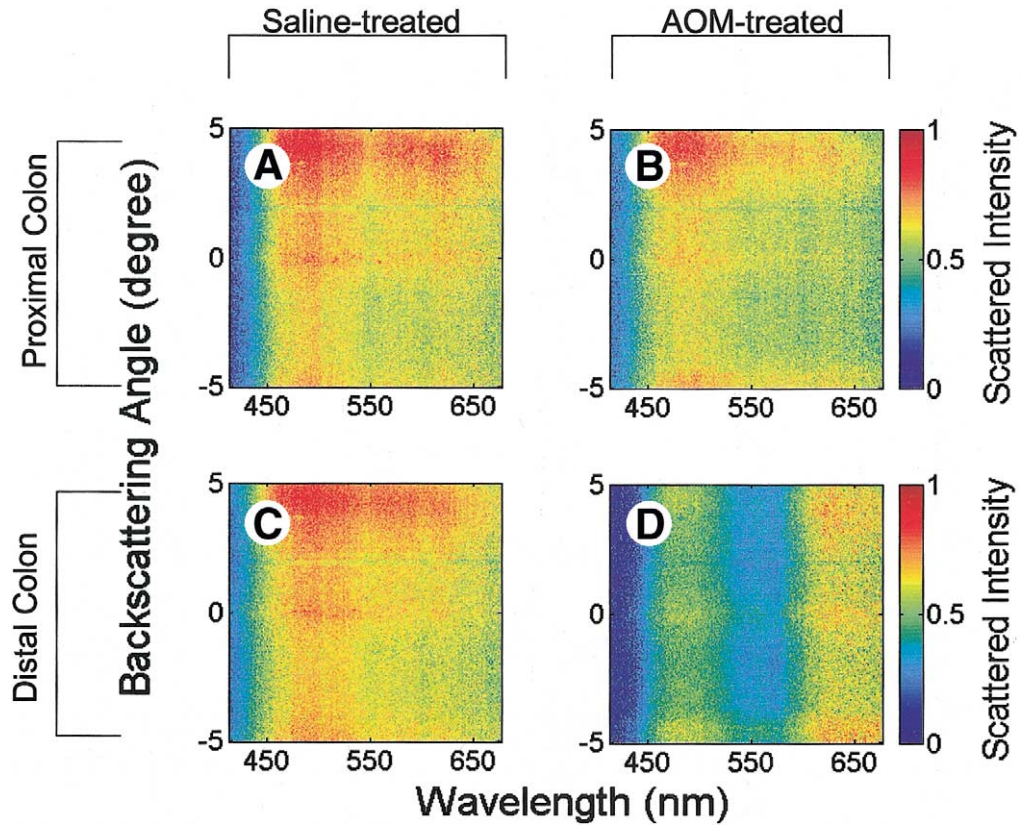

Figure 3. Representative 4D-ELF fingerprints from rats killed 2 weeks after injection of AOM or saline. The color represents intensity of backscattering light. The horizontal axis is the wavelength of the backscattering light. The vertical axis is the backscattering angle. (*A*) Saline-treated rat, proximal colon; (*B*) AOM-treated rat, proximal colon; (*C*) saline-treated rat, distal colon; (*D*) AOM-treated rat, distal colon. As shown, even at this very early time point, treatment with AOM had a dramatic effect on 4D-ELF signatures in the distal colon. However, in the proximal colon, the changes attributable to treatment with AOM were quite subtle.

less numerous than distal ACF. No ACF were detected in the saline-treated animals.

Overview of 4D-ELF Analysis

To analyze the signatures, we assayed a variety of parameters that span the spectrum of microarchitectural abnormalities. Fingerprint analysis gives a dramatic, albeit qualitative, appreciation of AOM-induced alterations. The spectral slope analysis evaluates size distribution of particles ranging from macromolecules to organelles. Fractal dimension, on the other hand, reflects alterations of the tissue organization at much larger scales, ranging from large organelles to groups of cells. PCA is a standard data procedure for assessing underlying structure in a data set. To infer a relationship to colon carcinogenesis, we correlated the 4D-ELF signatures with the subsequent occurrence of ACF. Specifically, neoplastic signatures should progress over time and be predominantly in the distal colon, especially early during carcinogenesis (mirroring our ACF data). All data from AOM-related signatures were compared with an age-matched saline-treated rat.

Elastic Light-Scattering Fingerprints

4D-ELF data obtained from each point on a tissue surface have 4 dimensions: wavelength λ, scattering angle θ, azimuth of scattering ϕ, and polarization of scattered light. These 4-dimensional data provide the most complete representation of the scattering properties of a tissue. Moreover, these 4-dimensional fingerprints are extremely sensitive to changes in tissue organization at scales ranging from nanometers ($\sim$30–40 nm) to tens of microns (see following text).[20]

Figure 3 shows representative light-scattering fingerprints recorded from a rat at an early stage of carcinogenesis (2 weeks after carcinogen treatment) and a control animal (2 weeks after saline treatment). For the control (saline-treated) animal, there are slight differences between the back-scattering intensity (especially at larger back-scattering angles) as indicated by subtle changes in color intensity recorded from proximal (Figure 3*A*) and distal (Figure 3*C*) colons, respectively. This finding is consistent with our understanding of the biological differences in the regions of the colon. Moreover, in the proximal colon (Figure 3*B*), treatment with AOM induced modest changes in the light-scattering fingerprints (most notably at the longer wavelengths) compared with corresponding fingerprints from control animals (Figure 3*A*). This finding is consistent with the minimal carcinogenic effect of AOM in the proximal colon, which is supported by data from our group and

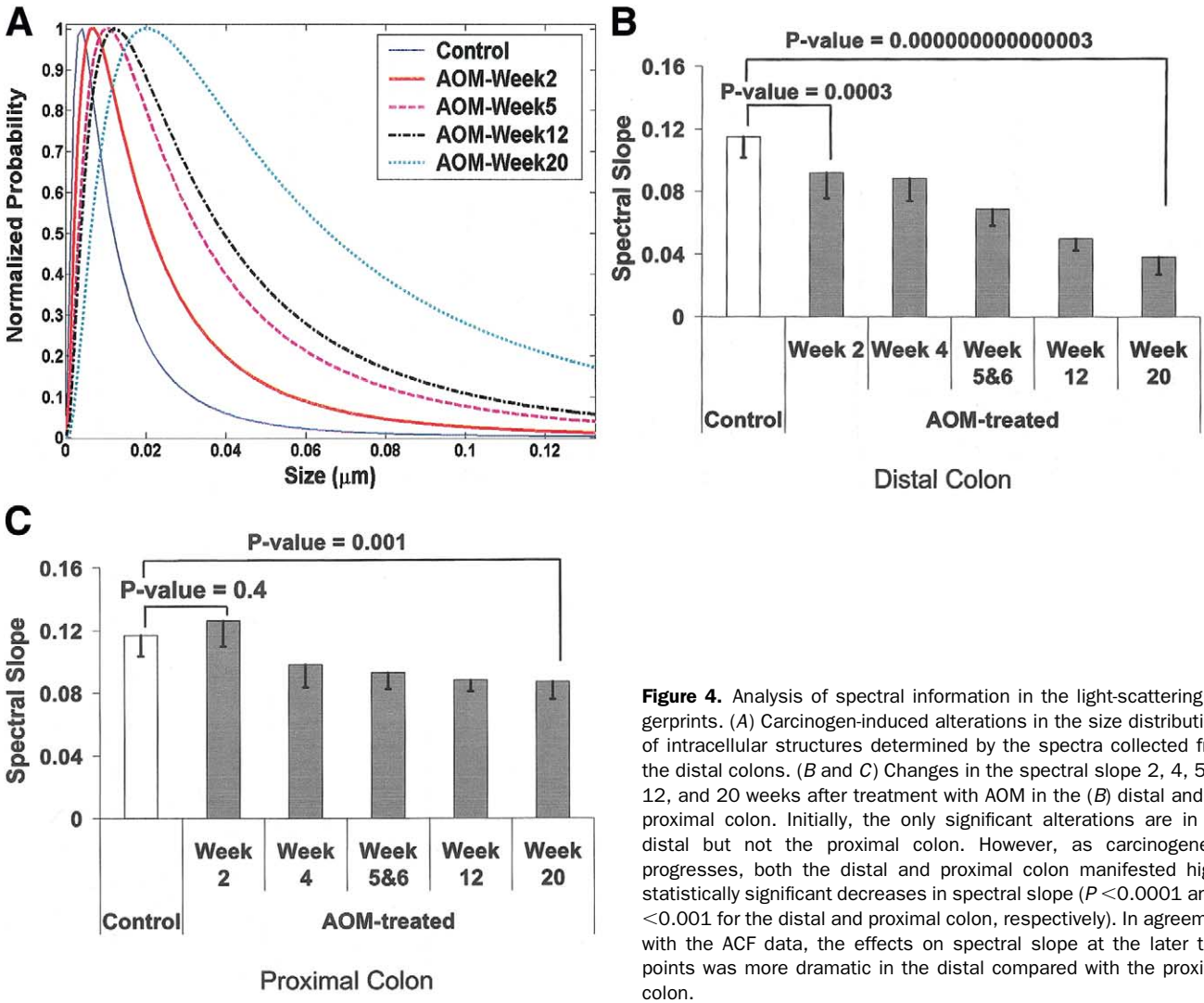

Figure 4. Analysis of spectral information in the light-scattering fingerprints. (*A*) Carcinogen-induced alterations in the size distributions of intracellular structures determined by the spectra collected from the distal colons. (*B* and *C*) Changes in the spectral slope 2, 4, 5, 6, 12, and 20 weeks after treatment with AOM in the (*B*) distal and (*C*) proximal colon. Initially, the only significant alterations are in the distal but not the proximal colon. However, as carcinogenesis progresses, both the distal and proximal colon manifested highly statistically significant decreases in spectral slope ($P < 0.0001$ and $P < 0.001$ for the distal and proximal colon, respectively). In agreement with the ACF data, the effects on spectral slope at the later time points was more dramatic in the distal compared with the proximal colon.

others.[21] However, in the distal colon, the AOM-induced alterations of the fingerprints were much more dramatic (Figure 3*D* vs. 3*C*), paralleling the increased carcinogenic efficacy in this region of the colon. We noted that the time point for which the alteration of light-scattering fingerprints was detected (i.e., 2 weeks after treatment with AOM) preceded the formation of ACF or other previously described conventional biomarkers.

Spectral Analysis

In the present study, we focused on the analysis of the light-scattering fingerprint data in 2 dimensions: wavelength and scattering angle. As discussed in Materials and Methods, the light-scattering spectra $\Delta I(\lambda)$ were used to obtain information about the size distribution of submicron intraepithelial structures in the size range from 40 to 800 nm (i.e., from macromolecular complexes to organelles). Figure 4*A* shows representative size distribution curves obtained from distal colon tissue sites of control and AOM-treated animals at 2, 5, 12, and 20 weeks after the carcinogen treatment, respectively. As carcinogenesis progressed, a variety of parameters (i.e., mean size, probable size, and relative proportion of larger structures) indicated an increase in particle dimensions. These findings are indicative of profound changes in the cellular nanoscale organization at an early stage of neoplastic transformation. Such alteration of cell nanoarchitecture has not been previously reported, most likely due to methodological limitations. Thus, 4D-ELF–detected microarchitectural evaluation in situ represents a major technological advance with potentially important biological and clinical ramifications.

Spectral behavior of $\Delta I(\lambda)$ depends on the size distribution of scattering structures. Generally, $\Delta I(\lambda)$ is a declining function of wavelength and its steepness is related to the relative portion of structures of different

sizes. Typically, larger structures tend to reduce the steepness of the decline of $\Delta I(\lambda)$, whereas smaller scatterers tend to make $\Delta I(\lambda)$ decrease with steeper wavelength. To analyze the data and characterize the spectral variations of $\Delta I(\lambda)$, we obtained linear fits to $\Delta I(\lambda)$ using linear regression analysis. The absolute value of the linear coefficient of the fit (in all measurements, the linear coefficient is negative due to the decrease of ΔI with wavelength), which is referred hereafter to as the spectral slope, quantifies the dependence of the scattering spectrum on wavelength and may serve as an easily measurable marker to characterize the distribution of structures within the cells.

Figure 4*B* and *C* show alterations of the spectral slope in the AOM-treated rats compared with its control values. In the proximal colon, treatment with AOM failed to induce changes in the spectral slope at 2 weeks after the carcinogen treatment ($P = 0.43$). This finding is consistent with only minimal carcinogenic effect of AOM in the proximal colon. On the contrary, in the distal colon, the spectral slope is dramatically decreased as early as 2 weeks after carcinogen treatment ($P = 0.0003$) and continued to decrease over the course of the experiment ($P < 0.0001$). Such progressive and highly statistically significant alteration of the spectral slope indicates that this parameter can be used as a marker for early precancerous transformations and its change is not due to the acute action of AOM.

Fractal Dimension

The angular distributions of the scattered light were used to calculate the fractal dimensions of the tissue microarchitecture. The angular distribution $\Delta I(\theta)$ at 550 nm for each tissue site was Fourier transformed to yield the 2-point mass density correlation function $C(r) = (\rho[r]\,\rho[r' + r])$, where $\rho[r]$ is a local mass density at point r, which is proportional to the concentration of intracellular solids such as proteins, lipids, and DNA.[20,31,34] $C(r)$ quantifies the correlation between local tissue regions separated by distance r. For example, in a perfect solid, $C(r)$ is a constant. On the other hand, for an object composed of randomly distributed material, $C(r)$ vanishes rapidly with distance. We found that at all tissue sites, $C(r)$ closely followed a power-law for several decades of r ranging from ~1 to 50 μm. Such power-law density correlation functions have been extensively studied and are characteristic of a fractal-like or statistically self-similar organization. The general form of such $C(r)$ is r^{D-3}, where D is referred to as fractal dimension.[34] We obtained D from the linear slopes of $C(r)$ in the linear regions of log-log scale.

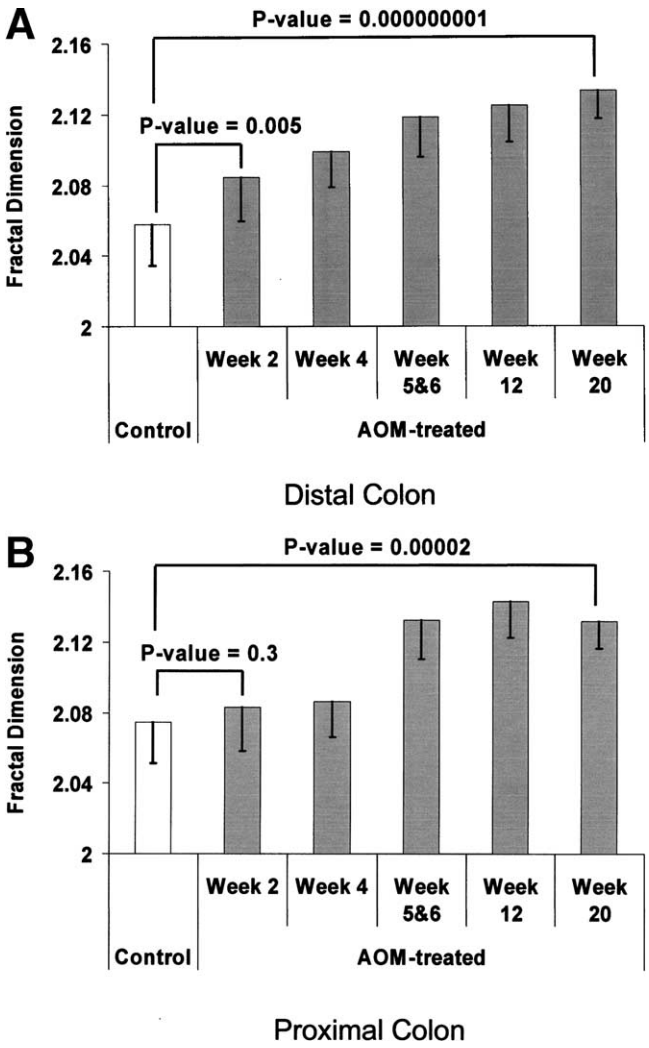

Figure 5. Analysis of scattering angle-dependent information in the light-scattering fingerprints through quantitation of the fractal dimension of the superficial mucosa. At the initial stages of carcinogenesis, fractal dimension significantly increased in the distal but not the proximal colon. However, as carcinogenesis progresses, both the distal and proximal colon manifested highly statistically significant increases in fractal dimension ($P < 0.0001$ for both the distal and proximal colon, respectively). However, consonant with the ACF and spectral slope data, the effects on fractal dimension at the later time points were more dramatic in the distal compared with the proximal colon.

As shown in Figure 5*A*, in the distal colon, fractal dimension was noted to be elevated as early as week 2 ($P = 0.005$) and continued to markedly increase over time ($P < 0.0001$). On the other hand, in the proximal colon, treatment with AOM failed to induce statistically significant alterations in fractal dimension. However, fractal dimension increased at later time points, albeit more modestly than that noted in the distal colon (Figure 5*B*).

PCA

PCA was performed as discussed in Materials and Methods. We first determined which principal component

Figure 6. PCA of light-scattering fingerprints: score of PC1 obtained from ELF collected for control and AOM-treated distal colon tissues at 2, 5, 6, 12, and 20 weeks after injection of carcinogen ($P = 5 \times 10^{-43}$). There was a minimal increase in PC1 in the proximal colon (data not shown).

was of interest. Typically in PCA, the first few principal components are responsible for most of the signal variations and the significance of higher-order principal components diminishes.[37] We found that, in our data, principal component 1 (PC1) accounted for ~99.3% of the data variance. Thus, PC1 is a convenient means to characterize the light-scattering fingerprint data. As shown in Figure 6, PC1 was significantly increased at 2 weeks in the distal colon ($P = 2 \times 10^{-12}$) and this progressively continued over the course of the experiment ($P = 5 \times 10^{-43}$). On the other hand, PC1 was minimally elevated in the proximal colon (data not shown).

Intersegment Variability

In our protocol, each colonic segment had at least 4 distinct 1-mm^2 areas probed. To assess whether 4D-ELF could have a clinical role, it is of considerable importance to determine the number of measurements required to reliably detect premalignancy. We established thresholds for categorizing an area as preneoplastic using PC1, linear slope, and fractal dimension. We analyzed sensitivity and specificity by applying these criteria to AOM- and saline-treated animals, respectively. Using this set of parameters, even at the earliest time point (2 weeks after injection of AOM), 90% of areas probed in the distal colon would correctly classify the animal as being exposed to carcinogen. This improved to 100% as the effects of the carcinogen progressed (weeks 12 and beyond). The specificity for all time points was 100%. This suggests that even at the earliest stages of colon carcinogenesis (2 weeks after treatment with AOM), 4 readings per colonic segment would provide a 99.99% probability of correctly diagnosing premalignancy. This accuracy far exceeds the capabilities of any conventional biomarker.

Discussion

Exploitation of the field effect in colon carcinogenesis is a common theme in colon cancer screening. As previously discussed, present strategies lack sufficient sensitivity and specificity for optimal population screening. For instance, although flexible sigmoidoscopy is a well-established and widely used screening technique, the problems with this test are underscored by the observation that less than one half of subjects with advanced proximal colon adenomas would also harbor lesions in the sigmoid and rectum.[40] Therefore, flexible sigmoidoscopy would not trigger colonoscopy in these cases and the proximal lesions would have the opportunity to evolve into invasive carcinomas. Thus, the finding of an accurate marker for the field effect would be of major clinical importance.

Application of the newly developed 4D-ELF has great promise for colon cancer screening because of the remarkable sensitivity to the earliest changes in carcinogenesis. Using quantitative analysis of tissue microarchitecture, we were able to detect the earliest alterations in neoplastic transformation (at 2 weeks after carcinogen treatment), which may reflect the field effect. The relevance of these 4D-ELF changes to carcinogenesis is supported by both the temporal and spatial correlation. Temporally, the marked alterations detected at week 2 progressively increased in magnitude over time consonant with the neoplastic effects of AOM in this model. Spatially, the early signature alterations were predominantly in the distal colon, the region of the colon most susceptible to ACF and tumor development. Moreover, the changes noted with 4D-ELF occurred at 2 weeks after treatment with AOM, a time point far earlier than seen with other conventional biomarkers. This time point was of particular importance in that the nonspecific genetic and cellular changes associated with acute carcinogen administration have dissipated.[41] Therefore, alterations at this time reflect the earliest changes related to the field effect of carcinogenesis. The biological plausibility of the heretofore-undescribed microarchitectural changes is supported by several recent reports cataloging genetic changes in colon carcinogenesis. Indeed, one study reported that 4 weeks after treatment with AOM, a decrease in APC message was detectable with a concomitant increase in cyclooxygenase 2 and c-myc expression.[42] Although the architectural consequences of these genetic alterations were not explored, APC, c-myc, and cyclooxygenase 2 have been reported to alter cellular structure and function.

We believe our data provide compelling evidence that the microarchitectural perturbations in the histologically

normal mucosa identified by 4D-ELF represent a reliable marker of the field effect of colon carcinogenesis. However, as opposed to classic definitions of field effect, the alterations we noted occurred before onset of frank neoplasia. This could potentially have great clinical utility by accurately identifying individuals at future risk of developing colorectal cancer. An unlikely alternative explanation is that 4D-ELF may actually be detecting early dysplastic areas in uninvolved colonic mucosa such as ACF or β-catenin–filled crypts.[43] However, it is implausible that our findings simply reflect a more sensitive methodology for detecting these conventional early dysplastic lesions. Early during carcinogenesis (<10 weeks after injection of AOM), ACF and β-catenin crypts are relatively infrequently interspersed throughout the distal colon and yet we noted diagnostic abnormalities in 90% of areas assayed at 2 weeks and 100% at 12 weeks after carcinogen treatment. Moreover, we were unable to detect any ACF 2 weeks after injection of AOM, further arguing against the proposition that we were simply detecting dysplastic areas. However, it is possible that 4D-ELF may be detecting previously undescribed preneoplastic lesions, although such putative lesions would have to be remarkably abundant.

The microarchitectural changes that we noted early in colon carcinogenesis encompassed a large spectrum of parameters. Our results indicate that the size distribution of submicron intraepithelial structures shifts toward larger sizes very early in carcinogenesis. Although the biological determinants of this phenomenon are unclear, it may reflect an increase in the sizes of macromolecular complexes (i.e., more protein-protein interactions). Fractal dimension, on the other hand, reflects changes in cell organization at much larger scales, ranging from large organelles to cells. Alterations in fractal dimension have been postulated to be one of the earliest changes in colon cancer.[44] The most common way of measuring fractal dimension is through box-counting approximations, which would clearly not be practical for colon cancer screening.[45] Using 4D-ELF, we are able to measure this parameter rapidly and accurately. We envision that, in the future, clinical determinations of fractal dimension and other microarchitectural parameters could be achieved through use of a probe compatible with a flexible sigmoidoscope (or colonoscope). This information could potentially be used to quantitate an individual's risk for developing colorectal neoplasms and therefore determine the most appropriate methodology and frequency for colorectal cancer screening.

The voluminous data generated by 4D-ELF were also analyzed through PCA. PCA has been used for many biological/clinical purposes, including both assessment of karyotypic alterations[46] and distinct biological features (e.g., global molecular phenotype)[47] in human colon cancer. This variable reduction procedure is useful in assessing underlying structure in a complex data set. Because principal components are extracted in a stepwise fashion, the first principal component is responsible for the largest amount of the variance.[48] We show that PC1 is a powerful discriminator between saline- and AOM-treated mucosa. This is of potentially great clinical significance in that this marker of the field effect may be exploited for colorectal cancer screening in the future. Moreover, it is important to note that despite the extensive "data mining" performed on 4D-ELF signatures, this represents <5% of total information available. Therefore, it is conceivable that our remarkable findings of early changes in carcinogenesis may be eclipsed by future ELF analyses.

Several other optical techniques have been used to detect cells undergoing neoplastic transformation. For instance, we and others have previously shown that LSS, the precursor technology to 4D-ELF, was able to detect cells in several human organs, including the colon, through evaluation of nuclear size and chromatin density.[15,17,30] Other bio-optics techniques (optical coherence tomography, Raman spectroscopy, angle-resolved low-coherence interferometry, and so on) have also been shown to be useful in detecting pathologically apparent dysplasia.[19,25,27,35,49] However, previous investigations using these techniques have focused on the diagnosis of more advanced, histologically apparent stages of neoplastic transformation and none of these techniques have been shown to allow identification of predysplastic epithelium.

The data obtained from light-scattering fingerprinting should not be considered a mere substitution for the morphologic tissue analysis using light microscopy. The 4-dimensional information extracted from ELF provides much greater biological insights than the previously used technologies. The critical advantages are related to the quantitative information regarding nanoscale architecture on living tissues. 4D-ELF gives information at the level of electron microscopy and yet keeps the levels of cellular organization that may be lost with staining/fixation, allowing heretofore-undiscovered insights regarding microarchitectural changes that occur early in neoplastic transformation. Given the complexity of the signatures, some signals may not allow direct correlation to a specific feature of the cellular architecture but still may serve as valuable intermediate biomarkers for carcinogenesis.

Although our data are compelling, caution always needs to be exercised when extrapolating findings from an exper-

imental model to humans. However, the AOM-treated rat is an established, robust, and well-validated model of human colon carcinogenesis. This model replicates the progression of the genetic, cellular, and morphologic events of human sporadic colon cancer. Furthermore, our preliminary studies using the other major experimental model, the multiple intestinal neoplasia mouse, also noted marked 4D-ELF alterations occurring at the pretumorigenic stage, dispelling the possibility that our findings are model specific (unpublished data, September 2003). Another caveat relates to the distal predominance seen in the AOM-treated rat. Although most human colon cancers are also located in the distal colon, there are increasing data suggesting that neoplasms that form in the proximal colon are quite distinct from those that form distally. For instance, proximal colon cancers have a much higher rate of microsatellite instability (25% vs. 2%), are more likely to occur in older and female patients, and, stage for stage, have a better prognosis than left-sided tumors.[50] Thus, the AOM-treated rat may not adequately represent the subset of human colon cancers that occur in the right colon. Nevertheless, epigenetic field changes are a hallmark of proximal cancers, as evident by the observation of frequent promoter hypermethylation in tumor-suppressor genes (including the DNA mismatch repair enzyme hMLH-1) in both right-sided colon cancers and the uninvolved mucosa.[51] Whether right-sided field changes will be detectable in the left colon remains to be determined. Our results in the AOM-treated rat indicate that 4D-ELF clearly identified changes in the colonic region distant from the predominant site of carcinogenesis (e.g., signatures in the proximal rat colon were also altered), suggesting that there should be distal microarchitectural correlates of proximal neoplasia.

In summary, this report shows that the newly developed technology 4D-ELF was able to detect heretofore-unrecognized subtle microarchitectural perturbations from the field effect of colon carcinogenesis. This technology has the promise of allowing accurate risk stratification and identifying patients who would benefit from colonoscopic screening and, of equal importance, determining who may not require intensive colorectal cancer screening. One can envision the rapid "bench-to-bedside" transition of this technology through the development of an endoscopically compatible probe with real-time signature determination. Moreover, 4D-ELF can give unparalleled insights into biological changes early in carcinogenesis. Further studies are being performed to translate this technology into clinical practice and to determine the biological determinants of these microarchitectural alterations.

References

1. Jemal A, Murray T, Samuels A, Ghafoor A, Ward E, Thun MJ. Cancer statistics, 2003. CA Cancer J Clin 2003;53:5–26.
2. Winawer S, Fletcher R, Rex D, Bond J, Burt R, Ferrucci J, Ganiats T, Levin T, Woolf S, Johnson D, Kirk L, Litin S, Simmang C. Colorectal cancer screening and surveillance: clinical guidelines and rationale—update based on new evidence. Gastroenterology 2003;124:544–560.
3. Zack DL, DiBaise JK, Quigley EMM, Roy HK. Colorectal cancer screening compliance by medicine residents: perceived and actual. Am J Gastroenterol 2001;96:3004–3008.
4. Sirovich BE, Schwartz LM, Woloshin S. Screening men for prostate and colorectal cancer in the United States—does practice reflect the evidence? JAMA 2003;289:1414–1420.
5. Braakhuis B, Tabor M, Kummer J, Leemans C, Brakenhoff R. A genetic explanation of slaughter's concept of field cancerization: evidence and clinical implications. Cancer Res 2003;63:1727–1730.
6. Lewis JD, Ng K, Hung KE, Bilker WB, Berlin JA, Brensinger C, Rustgi AK. Detection of proximal adenomatous polyps with screening sigmoidoscopy—a systematic review and meta-analysis of screening colonoscopy. Arch Intern Med 2003;163:413–420.
7. Takayama T, Katsuki S, Takahashi Y, Ohi M, Nojiri S, Sakamaki S, Kato J, Kogawa K, Miyake H, Niitsu Y. Aberrant crypt foci of the colon as precursors of adenoma and cancer. N Engl J Med 1998;339:1277–1284.
8. Martin C, Connelly A, Keku TO, Mountcastle SB, Galanko J, Woosley JT, Schliebe B, Lund PK, Sandler RS. Nonsteroidal anti-inflammatory drugs, apoptosis, and colorectal adenomas. Gastroenterology 2002;123:1770–1777.
9. Bernstein C, Bernstein H, Garewal H, Dinning P, Jabi R, Sampliner RE, McCuskey MK, Panda M, Roe DJ, L'Heureux L, Payne C. A bile acid-induced apoptosis assay for colon cancer risk and associated quality control studies. Cancer Res 1999;59:2353–2357.
10. McGarrity TJ, Peiffer LP. Protein-kinase-c activity as a potential marker for colorectal neoplasia. Dig Dis Sci 1994;39:458–463.
11. Vucenik I, Gotovac J, Druzijanic N, Shamsuddin AM. Usefulness of galactose oxidase-Schiff test in rectal mucus for screening of colorectal malignancy. Anticancer Res 2001;21:1247–1255.
12. Yoshikawa R, Utsunomiya J. Cell proliferation kinetics are abnormal in transitional mucosa adjacent to colorectal carcinoma. Br J Surg 1996;83:36–39.
13. Weyn B, Jacob W, da Silva VD, Montironi R, Hamilton PW, Thompson D, Bartels HG, Van Daele A, Dillon K, Bartels PH. Data representation and reduction for chromatin texture in nuclei from premalignant prostatic, esophageal, and colonic lesions. Cytometry 2000;41:133–138.
14. Montag AG, Bartels PH, Dytch HE, Lermapuertas E, Michelassi F, Bibbo M. Karyometric features in nuclei near colonic adenocarcinoma—statistical analysis. Anal Quant Cytol Histol 1991;13:159–167.
15. Backman V, Wallace MB, Perelman LT, Arendt JT, Gurjar R, Muller MG, Zhang Q, Zonios G, Kline E, McGillican T, Shapshay S, Valdez T, Badizadegan K, Crawford JM, Fitzmaurice M, Kabani S, Levin HS, Seiler M, Dasari RR, Itzkan I, Van Dam J, Feld MS. Detection of preinvasive cancer cells. Nature 2000;406:35–36.
16. Perelman LT, Backman V, Wallace M, Zonios G, Manoharan R, Nusrat A, Shields S, Seiler M, Lima C, Hamano T, Itzkan I, Van Dam J, Crawford JM, Feld MS. Observation of periodic fine structure in reflectance from biological tissue: a new technique for measuring nuclear size distribution. Phys Rev Lett 1998;80:627–630.
17. Gurjar RS, Backman V, Perelman LT, Georgakoudi I, Badizadegan K, Itzkan I, Dasari RR, Feld MS. Imaging human epithelial properties with polarized light-scattering spectroscopy. Nat Med 2001;7:1245–1248.
18. Wallace MB, Perelman LT, Backman V, Crawford JM, Fitzmaurice

M, Seiler M, Badizadegan K, Shields SJ, Itzkan I, Dasari RR, Van Dam J, Feld MS. Endoscopic detection of dysplasia in patients with Barrett's esophagus using light-scattering spectroscopy. Gastroenterology 2000;119:677–682.
19. Georgakoudi I, Jacobson BC, Van Dam J, Backman V, Wallace MB, Muller MG, Zhang Q, Badizadegan K, Sun D, Thomas GA, Perelman LT, Feld MS. Fluorescence, reflectance, and light-scattering spectroscopy for evaluating dysplasia in patients with Barrett's esophagus. Gastroenterology 2001;120:1620–1629.
20. Kim Y, Liu Y, Wali RK, Roy HK, Goldberg MJ, Kromine AK, Chen K, Backman V. Simultaneous measurement of angular and spectral properties of light scattering for characterization of tissue microarchitecture and its alteration in early precancer. IEEE J Sel Top Quantum Electron 2003;9:243–257.
21. Banerjee A, Quirke P. Experimental models of colorectal cancer. Dis Colon Rectum 1998;41:490–505.
22. Jacques SL, Roman JR, Lee K. Imaging superficial tissues with polarized light. Lasers Surg Med 2000;26:119–129.
23. Demos SG, Alfano RR. Optical polarization imaging. Appl Optics 1997;36:150–155.
24. Zonios G, Perelman LT, Backman VM, Manoharan R, Fitzmaurice M, Van Dam J, Feld MS. Diffuse reflectance spectroscopy of human adenomatous colon polyps in vivo. Appl Optics 1999;38: 6628–6637.
25. Bigio IJ, Mourant JR. Ultraviolet and visible spectroscopies for tissue diagnostics: fluorescence spectroscopy and elastic-scattering spectroscopy. Phys Med Biol 1997;42:803–814.
26. Lin WC, Toms SA, Jansen ED, Mahadevan-Jansen A. Intraoperative application of optical spectroscopy in the presence of blood. IEEE J Sel Top Quantum Electron 2001;7:996–1003.
27. Drezek R, Guillaud M, Collier T, Boiko I, Malpica A, Macaulay C, Follen M, Richards-Kortum R. Light scattering from cervical cells throughout neoplastic progression: influence of nuclear morphology, DNA content, and chromatin texture. J Biomed Opt 2003;8:7–16.
28. Yodh AG, Chance B. Spectroscopy and imaging with diffusing light. Physics Today 1995;48:34–40.
29. Tromberg BJ, Shah N, Lanning R, Cerussi A, Espinoza J, Pham T, Svaasand L, Butler J. Non-invasive in vivo characterization of breast tumors using photon migration spectroscopy. Neoplasia 2000;2:26–40.
30. Backman V, Gurjar R, Badizadegan K, Itzkan L, Dasari RR, Perelman LT, Feld MS. Polarized light scattering spectroscopy for quantitative measurement of epithelial cellular structures in situ. IEEE J Sel Top Quantum Electron 1999;5:1019–1026.
31. Backman V, Gopal V, Kalashnikov M, Badizadegan K, Gurjar R, Wax A, Georgakoudi I, Mueller M, Boone CW, Dasari RR, Feld MS. Measuring cellular structure at submicrometer scale with light scattering spectroscopy. IEEE J Sel Top Quantum Electron 2001; 7:887–893.
32. Schmitt JM, Kumar G. Optical scattering properties of soft tissue: a discrete particle model. Appl Optics 1998;37:2788–2797.
33. Borse GJ. Fortran 77 and numerical methods for engineers. Boston, MA: PWS-KENT, 1991.
34. Wax A, Yang CH, Backman V, Badizadegan K, Boone CW, Dasari RR, Feld MS. Cellular organization and substructure measured using angle-resolved low-coherence interferometry. Biophys J 2002;82:2256–2264.
35. Wax A, Yang CH, Muller MG, Nines R, Boone CW, Steele VE, Stoner GD, Dasari RR, Feld MS. In situ detection of neoplastic transformation and chemopreventive effects in rat esophagus epithelium using angle-resolved low-coherence interferometry. Cancer Res 2003;63:3556–3559.
36. Mourant JR, Fuselier T, Boyer J, Johnson TM, Bigio IJ. Predictions and measurements of scattering and absorption over broad wavelength ranges in tissue phantoms. Appl Optics 1997;36:949–957.
37. Dillon WR, Goldstein M. Multivariate analysis: methods and applications. New York: Wiley, 1984.
38. Ramanujam N, Mitchell MF, Mahadevan A, Thomsen S, Malpica A, Wright T, Atkinson N, Richards-Kortum R. Development of a multivariate statistical algorithm to analyze human cervical tissue fluorescence spectra acquired in vivo. Lasers Surg Med 1996;19:46–62.
39. Roy HK, Karolski WJ, Ratashak A. Distal bowel selectivity in the chemoprevention of experimental colon carcinogenesis by the non-steroidal anti-inflammatory drug nabumetone. Int J Cancer 2001;92:609–615.
40. Lieberman DA, Weiss DG, Bond JH, Ahnen DJ, Garewal H, Chejfec G, Harford WV, Provenzale D, Sontag S, Schnell T, Campbell DR, Durbin TE, Nelson DB, Ewing SL, Triadafilopoulos G, Ramirez FC, Lee JG, Collins JF, Fennerty B, Johnston TK, Corless CT, McQuaid KR, Sampliner RE, Morales TG, Fass R, Smith R, Maheshwari Y. Use of colonoscopy to screen asymptomatic adults for colorectal cancer. Veterans Affairs Cooperative Study Group 380. N Engl J Med 2000;343:162–168.
41. Jackson PE, O'Connor PJ, Cooper DP, Margison GP, Povey AC. Associations between tissue-specific DNA alkylation, DNA repair and cell proliferation in the colon and colon tumour yield in mice treated with 1,2-dimethylhydrazine. Carcinogenesis 2003;24:527–533.
42. Kishimoto Y, Morisawa T, Hosoda A, Shiota G, Kawasaki H, Hasegawa J. Molecular changes in the early stage of colon carcinogenesis in rats treated with azoxymethane. J Exp Clin Cancer Res 2002;21:203–211.
43. Yamada Y, Mori H. Pre-cancerous lesions for colorectal cancers in rodents: a new concept. Carcinogenesis 2003;24:1015–1019.
44. Waliszewski P, Molski M, Konarski J. On the holistic approach in cellular and cancer biology: nonlinearity, complexity, and quasi-determinism of the dynamic cellular network. J Surg Oncol 1998; 68:70–78.
45. Roy HK, Lynch HT. Diagnosing Lynch syndrome: is the answer in the mouth? Gut 2003;52:1665–1667.
46. Hoglund M, Gisselsson D, Hansen GB, Sall T, Mitelman F, Nilbert M. Dissecting karyotypic patterns in colorectal tumors: two distinct but overlapping pathways in the adenoma-carcinoma transition. Cancer Res 2002;62:5939–5954.
47. Mori Y, Selaru FM, Sato F, Yin J, Simms LA, Xu Y, Olaru A, Deacu E, Wang S, Taylor JM, Young J, Leggett B, Jass JR, Abraham JM, Shibata D, Meltzer SJ. The impact of microsatellite instability on the molecular phenotype of colorectal tumors. Cancer Res 2003; 63:4577–4582.
48. Hoglund M, Gisselsson D, Sall T, Mitelman F. Coping with complexity: multivariate analysis of tumor karyotypes. Cancer Genet Cytogenet 2002;135:103–109.
49. Van Dam J. Novel methods of enhanced endoscopic imaging. Gut 2003;52:12–16.
50. Iacopetta B. Are there two sides to colorectal cancer? Int J Cancer 2002;101:403–408.
51. Jass JR, Whitehall VLJ, Young J, Leggett BA. Emerging concepts in colorectal neoplasia. Gastroenterology 2002;123:862–876.

Received September 28, 2003. Accepted December 29, 2003.

Address requests for reprints to: Hemant K. Roy, M.D., Feinberg School of Medicine at Northwestern University, Evanston Northwestern Healthcare Research Institute, 1001 University Place, Evanston, Illinois 60201. e-mail: h-roy@northwestern.edu; fax: (847) 570-8011.

Supported by research grants from the National Institutes of Health (1R21CA102750-01), National Science Foundation (BES-0238903), General Motors Cancer Research Foundation, and American Cancer Society/Illinois Division.

Presented in part in abstract form at the 104th Digestive Disease Week meetings, May 17–21, 2003, in Orlando, Florida (Gastroenterology 2003;124(Suppl 1):A5).